



HAL
open science

Water-soluble/visible-light-sensitive naphthalimide derivative-based photoinitiating systems: 3D printing of antibacterial hydrogels

Hong Chen, Laurent Pieuchot, Pu Xiao, Frédéric Dumur, Jacques Lalevée

► To cite this version:

Hong Chen, Laurent Pieuchot, Pu Xiao, Frédéric Dumur, Jacques Lalevée. Water-soluble/visible-light-sensitive naphthalimide derivative-based photoinitiating systems: 3D printing of antibacterial hydrogels. *Polymer Chemistry*, 2022, 13 (20), pp.2918-2932. 10.1039/d2py00417h . hal-03677750

HAL Id: hal-03677750

<https://hal.science/hal-03677750>

Submitted on 24 May 2022

HAL is a multi-disciplinary open access archive for the deposit and dissemination of scientific research documents, whether they are published or not. The documents may come from teaching and research institutions in France or abroad, or from public or private research centers.

L'archive ouverte pluridisciplinaire **HAL**, est destinée au dépôt et à la diffusion de documents scientifiques de niveau recherche, publiés ou non, émanant des établissements d'enseignement et de recherche français ou étrangers, des laboratoires publics ou privés.

Water-soluble/visible-light-sensitive naphthalimide derivative-based photoinitiating systems: 3D printing of antibacterial hydrogels

Hong Chen ^{1,2}, Laurent Pieuchot ^{1,2}, Pu Xiao ^{3*}, Frédéric Dumur ^{4*} and Jacques Lalevée ^{1,2,*}

¹ Université de Haute-Alsace, CNRS, IS2M UMR 7361, F-68100 Mulhouse, France;

² Université de Strasbourg, France

³ Research School of Chemistry, Australian National University, Canberra ACT 2601, Australia

⁴ Aix Marseille Univ, CNRS, ICR UMR 7273, F-13397 Marseille, France

* Correspondance: pu.xiao@anu.edu.au (P.X.); frederic.dumur@univ-amu.fr (F.D.); jacques.lalevee@uha.fr (J.L.)

Abstract: Adaptability of hydrogels allows these structures to be used in a variety of industries, including biomedicine, soft electronics, and sensors. In this study, 10 different naphthalimide derivatives were synthesized, of which two naphthalimide salts with an excellent water solubility. These dyes could be used as high-efficiency water-soluble photoinitiators when combined with water-soluble co-initiator, namely arginine (L-Arg)/triethanolamine (TEA) as electron donors and an iodonium salt (Iod) used as an electron acceptor. Using a three-component photoinitiating system, antibacterial hydrogels containing silver nanoparticles could be prepared upon irradiation with a visible light source (LED@405nm). It thus enabled to respond to the growing demand for radiation-curable waterborne products such as hydrogels. These two compounds exhibited an excellent water solubility of at least 6% for dye 9 and up to 10% for dye 8 in deionized water, thus exceeding the solubility of typically photoinitiator Irgacure 2959 (I2959) used in water-based systems 12- to 20- fold. Real-time Fourier transform infrared (FTIR) spectroscopy proved that the three-component photoinitiating system based on naphthalimide potassium salts achieved more than 90% double bond conversions of the poly(ethylene glycol) diacrylate (PEG-DA) under LED@405nm irradiation, comparable to that obtained with conventional water-soluble photoinitiators. Using the proposed water-soluble

photoinitiators, 3D printing hydrogels could be prepared and introduction of silver nitrate into the solution enabled the salt to be reduced in situ into silver nanoparticles and to produce antibacterial hydrogels. Finally, *Escherichia coli* was selected to investigate the effect of the antibacterial activity of hydrogels containing different concentrations of AgNPs.

Keywords: Naphthalimide derivatives; visible light photoinitiation system; water-solubility; antibacterial activity.

1. Introduction

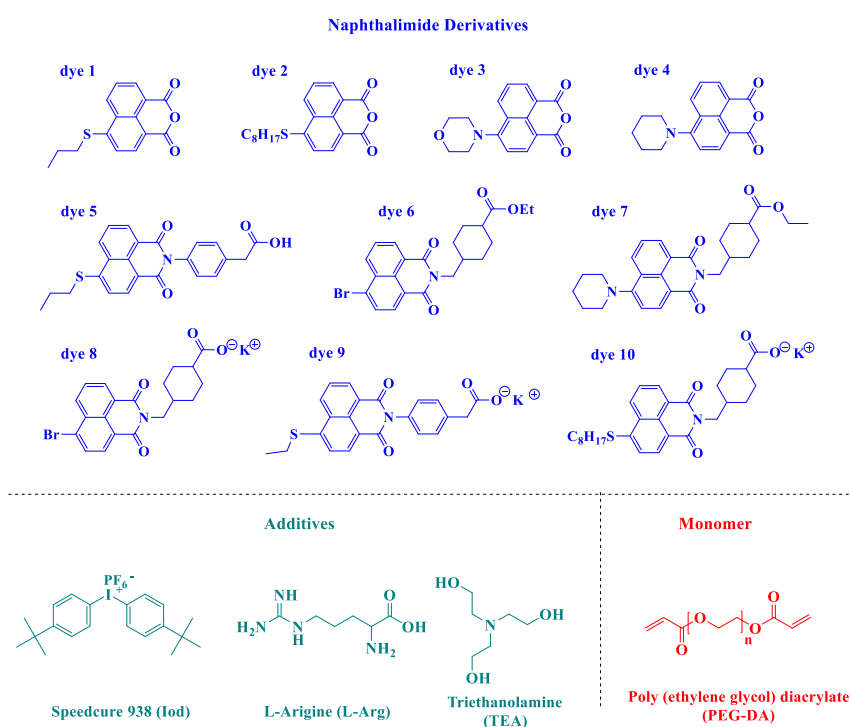
3D printing (also known as additive manufacturing) is a concurrent design and fabrication technique that combines materials, structures, and functions [1-2]. Due to its benefits of high accuracy, high efficiency, structural complexity and functional diversity, it has been successfully applied in industrial [3-4], medical [5-6], aviation [7], and educational domains [8-9] in recent years. Hydrogel is a three-dimensional (3D) network structure formed by cross-linking of hydrophilic polymer chains embedded into a water-rich environment with extensively adjustable physical and chemical properties, responding to the growing demand for radiation-curable waterborne products [10-12]. Therefore, hydrogel systems with pre-designed structures and functions can be prepared by 3D printing technology. Recent advances in the 3D printing of hydrogels have focused on the construction of tough, self-healing, cytocompatible hydrogel scaffolds with architectures that allow the generation of complex tissues [13-14]. Among other rapid prototyping techniques that may be utilized for 3D printed hydrogels, processing hydrogels with SLA-based 3D printing typically involves oligomers/reactive monomers and photoinitiators (PIs). Furthermore, moderate processing conditions such as the avoidance of heat, organic solvents, and ultraviolet (UV) exposure are essential for the manufacture of hydrogels embedded with living cells [15-16]. However, it is still challenging to develop effective water-soluble PIs that can overcome the aforementioned constraints.

Among the limited selection of commercially available water-soluble PIs, 2-hydroxy-4'-(2-hydroxyethyl)-2-methylpropiophenone (Irgacure 2959) is the most commonly used aqueous photoinitiator. Due to the limited solubility of this compound in water (~ 0.47 wt %), continuous stirring or moderate heating was required to fully dissolve them [17]. Noticeably, this photoinitiator has a low ability to initiate the

polymerization of hydrogels when exposed to light sources at wavelengths longer than 385 nm [18-19]. In addition, biocompatible riboflavin (Vitamin B₂) has also been reported as a water-soluble PI [20]. However, it can only be utilized in expensive two-photon polymerization printers with extremely tiny build sizes [21]. Furthermore, it also required a co-initiator (e.g. triethanolamine), nitrogen purge (particularly sensitive to oxygen), and high power input (>244 mW) [22-24]. Several studies have also shown that the riboflavin-triethanolamine mixture exhibited a lower photosensitivity than that achieved from the commercially available water-soluble PI (e.g. I2959) [21]. [Another highly efficient commercial water-soluble photoinitiator, TPO-Li, exhibits a significantly improved water solubility compared to that of I2959.](#) In addition, the [polymerization is very fast and double bond conversions of over 97% are achievable. photopolymerization efficiency of more than 95%.](#) However, this molecule [is only mainly sensitive to UV light, which is not conducive to the printing of hydrogels that involving living cells which](#) is a severe [limitation for the printing of hydrogels involving living cells](#) [25]. Therefore, there is an unmet need for highly efficient water-compatible PIs with high absorbance in the visible range to enable fast 3D printing of hydrogels.

Recently, we have reported on six naphthalimide derivatives used as efficient visible-light-sensitive photoinitiators in the combination of Iod and amine for free radical polymerization of acrylates and cationic polymerization of EPOX. However, only one naphthalimide sodium salt exhibited good water solubility, which can be used as a highly efficient water-soluble photoinitiator for the preparation of hydrogels. This encouraging result prompted us to explore further the possibility to prepare novel water-soluble naphthalimide derivatives with various substituents. [26] In this study, we designed and synthesized a series of naphthalimide derivatives modified with different functional groups, of which only two naphthalimide potassium salts (dyes 8 and 9) exhibited excellent water solubility. These two compounds were combined with aqueous co-initiators to form two- and three-component photoinitiating systems (PIS), and their photopolymerization efficiencies were investigated by real-time Fourier transform infrared spectroscopy upon irradiation with a LED@405 nm. After that, the involved redox mechanisms were investigated by combining several experiments such as photolysis and fluorescence quenching. The best PIS was chosen to initiate the photopolymerization of poly(ethylene glycol) diacrylate (PEG-DA) aqueous monomers while reducing the silver ions dispersed in the formulations into silver

nanoparticles. Due to the aqueous monomers used in this experiment, we evaluated the swelling properties of the produced hydrogels *via* rapid 3D printing using a low-cost SLA-based 3D printer without any organic solvents through two routes. Finally, *Escherichia coli* was selected to explore the effect of the antibacterial activity of PEG-hydrogels containing different concentrations of AgNPs.



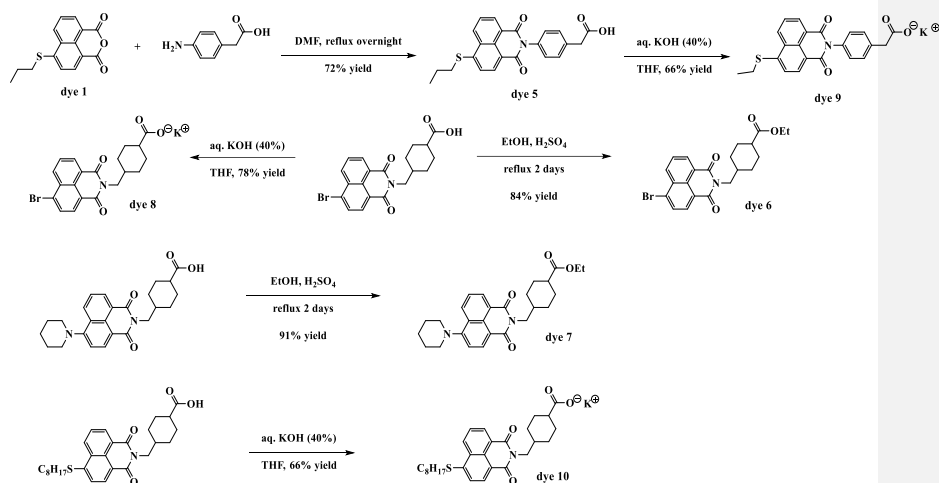
Scheme 1. Chemical structures of the naphthalimide derivatives used as PI, additives of Speedcure 938 (Iod), L-Arginine (L-Arg), Triethanolamine (TEA), and the functional benchmark monomer (PEG-DA) used in this work.

2. Materials and Methods

2.1. Chemical Compounds

The functional benchmark monomer used in this work, namely, poly(ethylene glycol) diacrylate (PEG-DA: SR 610) was purchased from Sartomer-Europe (Colombes). The water-soluble co-initiator triethanolamine and L-Arginine (TEA/L-Arg, used as an electron donor), as well as *bis*-(4-*tert*-butylphenyl)iodonium hexafluorophosphate (Iod, used as an electron acceptor) were all purchased from

Sigma-Aldrich (Saint-Quentin-Fallavier). Their molecular structures are shown in Scheme 1. The solvent (i.e. Dimethyl sulfoxide) was also purchased from Sigma-Aldrich and was of analytical grade. Naphthalimide derivatives were prepared as described in Supporting Information and their chemical structures are also shown in Scheme 1 (dyes 1-10). It has to be noticed that compounds 1, 2, 3, 4 and 10 were previously reported in the literature [27-31]. Compound 5 was synthesized in one step, by condensation of 6-(propylthio)-1*H*,3*H*-benzo[*de*]isochromene-1,3-dione (dye 1) with 4-aminophenylacetic acid, furnishing 2-(4-(1,3-dioxo-6-(propylthio)-1*H*-benzo[*de*]isoquinolin-2(3*H*)-yl)phenyl)acetic acid (dye 5) in 72% yield. By use of an aq. KOH solution, the anion of dye 5 could be prepared in 66% yield (dye 9). Dyes 8 and 6 were prepared from the same intermediate i.e. 4-((6-bromo-1,3-dioxo-1*H*-benzo[*de*]isoquinolin-2(3*H*)-yl)methyl)cyclohexane-1-carboxylic acid. By use of aqueous conditions, dye 8 could be obtained in 78% yield. Conversely, dye 6 was prepared in 84% yield by esterification of the corresponding acid. Finally, dye 7 and dye 10 were also obtained by esterification with ethanol using a catalytic amount of concentrated sulfuric acid. The two dyes i.e. dyes 7 and 10 were obtained in 91 and 66% yield respectively (See Scheme 2).



Scheme 2. Synthetic routes to dyes 5-10.

2.2. Water solubility of proposed naphthalimide derivatives.

The previous researches of our group have shown that some naphthalimide derivatives can be dissolved in water [31]. Therefore, in this work, 10 different naphthalimide derivatives were synthesized and used as visible light-sensitive photoinitiators. Water solubility of the ten dyes was investigated in deionized water and the best candidates were selected for the following studies.

2.3. Photopolymerization Experiments

Initiating ability of the one/two/three-component systems (dyes alone, dyes/Iod, dyes/TEA or L-Arg, dyes/Iod/TEA or L-Arg) comprising the selected water-soluble dyes was examined for an aqueous monomer (50% PEG-DA/50% water) and studied by real-time Fourier transform infrared spectroscopy (RT-FTIR, JASCO FTIR 4100, Lisses, France). Co-initiators TEA and L-Arg are hydrophilic substances that dissolve readily in an aqueous monomer, with the water solubility of TEA being greater than that of L-Arg. However, the iodonium salt also cannot dissolve in water, but the presence of PEG-DA allows it to be well-dispersed in an aqueous monomer. A visible light LED@405nm whose intensity is about 110 mW/cm² was used to initiate the polymerization of photosensitive formulations between two polypropylene (PP) films with a thickness of 0.1 mm or into molds (between two polypropylene films) with a thickness of 2 mm to reduce O₂ inhibition. The monitored peak is located around 1600 cm⁻¹ (thickness of about ~ 0.1 mm) or 6160 cm⁻¹ (thickness ~ 2 mm) [32].

2.4 Involved mechanism research

2.4.1 UV-Vis absorption properties of the selected dyes and their photolysis process and fluorescence quenching process with Iod and amine

A JASCO V730 spectrophotometer was used to study the UV-vis absorption properties of the proposed water-soluble dyes. Analyses were carried out in the water with a concentration of 5×10⁻³ wt%. As the iodonium salt is insoluble in water, photolysis of the dyes with Iod/amine and the dyes alone in DMSO was carried out using the JASCO V730 spectrophotometer, keeping the concentration of the water-soluble dyes at 5×10⁻³ wt%, while for the co-initiators (e.g. Iod and amine), concentrations were at about 1.5 wt% [33].

In addition, fluorescence spectra of the selected dyes were determined using a JASCO FP-6200 Spectro fluorimeter at a concentration of 5×10⁻³ wt% in water. Fluorescence quenching of the dyes with Iod or amine was carried out in DMSO at a

concentration of about 5×10^{-3} wt% and 1.5 wt%, respectively. The excitation wavelength was around 300~350 nm.

2.4.2 Electron spin resonance (ESR) spin trapping experiments (ESR-ST) and the free energy changes of dyes with Iod/amine

Radicals generated by the interactions between the proposed water-soluble dyes with Iod or amine under sunlight irradiation were trapped by PBN (0.25 wt%) in N_2 saturated DMSO solutions and then monitored using an X-band spectrometer (Bruker EMX-plus) at room temperature. Finally, the obtained ESR spectra were simulated and analyzed using WINSIM software [34].

Remarkably, the free energy changes (e.g. ΔG_{SI}^{Iod} or ΔG_{SI}^{EDB}) were calculated to detect the electron transfer reactions between the dyes and the additives (Iod/amine) and to support the experimentally observed photopolymerization processes. Redox potentials (E_{ox} and E_{red}) of the proposed dyes were determined by cyclic voltammetry in DMSO, and E^* , corresponding to the excited state energy level of the dyes, as determined by the intersection of their normalized UV-visible and fluorescence spectra.

2.5 Dynamic time sweep rheology and Tensile strength of the manufactured hydrogel.

Photopolymerization processes of all formulations were further examined by dynamic time-scan rheology. Specifically, 40 μ L of photosensitive resin was dropped on a glass slide and then measured at a constant frequency of 0.1 Hz at 25 °C using a Haake-Mars rotational rheometer with LED@405nm.

Tensile strength of the fabricated hydrogels (width ~4 mm, length ~50 mm, height ~2.5 mm) was measured using an Instron dynamometer at a displacement rate of 10 mm/min at room temperature until rupture. From the subsequent stress/strain curves, the final tensile strength and modulus of elasticity could be calculated. At least, three measurements were made for each specimen and the average value is reported [35].

2.6 Preparation of silver nanoparticles (AgNPs)

2.6.1 Preparation of AgNPs in DMF/ water using the proposed water-soluble PIS

DMF/water solutions containing 0.5 wt% three components PIS (dye/Iod/EDB) and 4 wt% silver nitrate were irradiated with visible light and their absorption spectra were measured at different times using a JASCO V730 spectrophotometer to confirm whether silver nanoparticles were produced under visible light irradiation [36].

2.6.2 Preparation of AgNPs in hydrogels

Hydrogels containing AgNPs were prepared by adding different proportions of AgNO₃ (1 wt%, 2 wt%, 4 wt%, and 8 wt%) in an aqueous monomer (50 wt% PEG-DA/50 wt% water), in which the dyes/Iod/amine (0.1 wt%/1.5 wt% 1.5 wt%)-based three-component PISs were completely dissolved. The resulting solutions were stirred at room temperature for 1 h to ensure that the salt was well distributed in the photosensitive formulations. Real-time FTIR spectroscopy was then used to track the monomer conversion, which not only allowed to examine the impact of the presence of the silver cations on the initiation ability of the proposed water-soluble PIS, but also allowed hydrogels containing different ratios of uniformly distributed silver nanoparticles to be prepared.

2.7 Applications in 3D and 4D.

2.7.1 Laser writing experiments to prepare hydrogels

Photosensitive formulations were prepared in aqueous monomer (50 wt% PEG-DA/50 wt% water), in which the proposed dye/Iod/amine-based PIS and/without metal salt (AgNO₃) were well distributed. Then, all direct laser writing experiments were successfully performed under air at room temperature using a SLA-based 3D printer with a laser diode at 405 nm (Thorlabs). Finally, topography and precision of the obtained 3D patterns were analyzed using a numerical optical microscope (DSX-HRSU from Olympus Corporation).

2.7.2 Swelling Experiments of the obtained hydrogels

Since the aqueous monomer contains 50% water, two approaches were used in this work to study the swelling properties of the resulting hydrogels. The first approach consisted in soaking the obtained hydrogels directly in deionized water at room temperature for 24 hours and then measuring their wet weight (Wt) and volume (V₁) after reaching swelling equilibrium. Then, the swollen hydrogels were heated in an oven at 40°C to remove the absorbed water, while their weight and volume were also measured. Another method consists in first heating the obtained hydrogels in an oven at 40°C to remove their internal moisture and then perform the subsequent swelling test according to the specific steps of the first method. The swelling ratio and volume change value of the obtained hydrogels were determined by comparing their wet weight

(Wt) and volume (V_1) values after reaching the swelling equilibrium with their initial values [37].

2.8 Antibacterial activity of hydrogels with different content of AgNPs.

To demonstrate the effect of different contents of AgNPs in hydrogels on the antibacterial activity, *Escherichia coli* was selected as a bacterial model in this work. PEG-hydrogel without AgNPs was used as a reference to systematically investigate the antibacterial activity of the obtained PEG-hydrogels with different content of AgNPs (1 wt%, 2 wt%, 4 wt%, 8 wt%). The bacterial strains were stored in 15% glycerol at -80 °C. The strains were cultured in LB medium (Lennox L: 1% bacto -tryptone, 0.5% bacto-yeast extract, 1% NaCl, NaOH [3×10^{-3} M]) at 37 °C. Prior to contact with the PEG-hydrogels, an overnight culture was established to start a new culture until $OD_{580nm} = 1$ (approximately 10^9 bacteria/ mL). 100 μ L is used to inoculate the new LB agar dish. After overnight growth in contact with PEG-hydrogels, the antibacterial activity was directly observed [38-39].

3. Results and Discussion

3.1 Water solubility of proposed naphthalimide-derivatives.

Since the previous work of our group has shown that some *naphthalimide*-derivatives have good water solubility, in this work, 10 different *naphthalimide*-derivatives were synthesized and used as photosensitive initiators. As can be seen in Figure 1, dyes 1, 2, 4, 6, and 7 were completely insoluble in water. Conversely, dyes 3, 5, and 10 were slightly soluble in water and their aqueous solutions were pale yellow and cloudy. Remarkably, dyes 8 and 9 were soluble in water as their solutions were yellow, clear, and transparent.

To confirm the solubility of these two dyes in water, concentration of these dyes in water was gradually increased. Figure S1 shows images of these two dyes in water at different concentrations from 0 to 10 wt% (more specifically 0.1 wt%, 1 wt%, 3 wt%, 5 wt%, 6 wt%, 7 wt%, 8 wt%, and 10 wt%). Color of the aqueous solution of dye 8 gradually deepened from colorless to yellow, and the solution remained clear and transparent until the concentration increased to 10%. For dye 9, the color of the aqueous solution also became darker as the concentration increased. However, the aqueous solution turned from clear to cloudy when the concentration increased from 6 to 7 wt%. It indicated that the solubility of dye 8 is higher than 10%, while 6 wt% may be close to

the saturation concentration for dye 9 in water, which is larger than that of the commercially available water-soluble photoinitiator (e.g. the solubility of I2959 is about 0.47 wt% [17]).

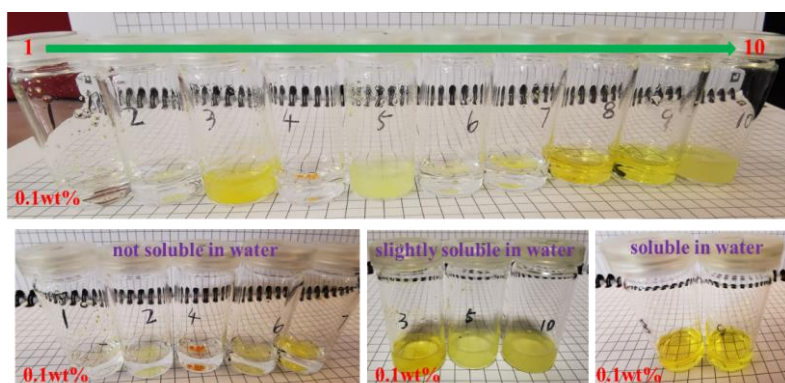


Figure 1. Images of 10 different dyes based on naphthalimide-derivatives in water at a concentration of 0.1 wt%.

3.2. Photopolymerization efficiency of the proposed water-soluble dyes based PIS

Photoinitiation ability of dyes 8 and 9 in combination with additives (Iod, TEA/L-Arg) as photoinitiating systems was investigated under visible light LED@405nm irradiation in laminate. Polymerization profiles of the aqueous monomer PEG-DA (50 wt% PEG-DA/50 wt% water) are depicted in Figure 2, deep curing cannot be observed in the formulations containing only dyes 8 or 9. After the addition of co-initiators or additives, initiation ability of the dye-based two-component PIS (Dye-Iod, Dye-TEA, and Dye-L-Arg) was improved so that a deep-curing could now occur at a thickness of about 2 mm. While for thin films of about 0.1 mm, except for dye 8 with the TEA/L-Arg based formulation, all other resins could also be polymerized to form hydrogels.

To further improve the efficiency of the free radical photopolymerization of waterborne monomer PEG-DA, a co-initiator Iod and an additive TEA/L-Arg were added and combined with the water-soluble dyes to form a three-component photoinitiating system (dye-Iod-TEA/dye-Iod-L-Arg). Although Iod is insoluble in water, they were fully dispersed in the resins in the presence of PEG-DA. As shown in Figure 2, **dye 9-Iod-TEA based** three-component PIS achieved the best polymerization efficiency including higher final acrylate functional conversion (about 97% for thick

films and 71% for thin films) and higher polymerization rate (the slope of the polymerization curves). In addition, all of them can be deeply cured within 100 s of light exposure.

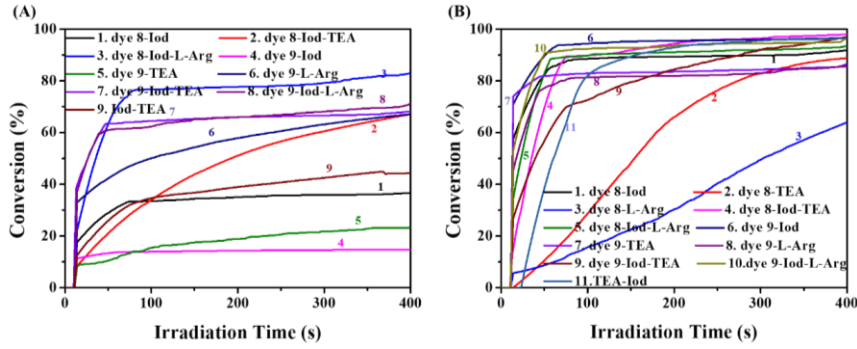


Figure 2. Photopolymerization kinetics (conversion of acrylate function vs. time) of the aqueous monomer PEG-DA (50 wt% PEG-DA/50 wt% water) initiated by dyes 8/9 based one/two/three-component photoinitiating systems (dyes, dye-Iod, dye-TEA/L-Arg, dye-Iod-TEA/L-Arg) in the laminate upon irradiation with a LED @ 405 nm with a thickness of (A) 0.1 mm and (B) 2 mm. The irradiation starts at $t = 10$ s.

Final Function Conversions of Waterborne Monomers (50%PEG-DA-50% Water)				
	Dye 8		Dye 9	
	Thin	Thick	Thin	Thick
Dye	-	-	-	-
Dye-Iod	37	92	15	96
Dye-TEA	-	89	23	87
Dye-L-Arg	-	64	67	86
Dye-Iod-TEA	67	98	67	97
Dye-Iod-L-Arg	83	94	71	97
Iod-TEA	45	96	45	96

“-” means no deep-curing can be observed

Table 1. Summary of the final function conversions of aqueous monomers (50 wt% PEG-DA/50 wt% water) at LED @ 405 nm initiated by dyes 8/9 based one/two/three-component photoinitiating systems (dyes, dye-Iod, dye-TEA/L-Arg,

dye-Iod-TEA/L-Arg) in laminate upon irradiation with a LED @ 405 nm having a thickness of about 0.1 and 2 mm.

3.3. Investigation of the mechanism involved.

Absorption property of the selected water-soluble dyes 8 and 9 was investigated in water and the corresponding spectra are presented in Figure 3. It is obvious that the extinction coefficients of these two dyes around 405 nm are both low (see Table S1, $9150 \text{ M}^{-1} \text{ cm}^{-1}$ for dye 9 and $4280 \text{ M}^{-1} \text{ cm}^{-1}$ for dye 8), and the maximum absorption peak of dye 8 appeared around 300 nm. Only the maximum absorption peak of dye 9 appeared at about 400 nm, which guarantees a good overlap with the emission spectrum of the LED@405 nm used in this work. It is evident that both dyes 8 and 9 have a relatively broad absorption range, from around 270–550 nm, which guarantees a good overlap with the emission spectrum of the LED@405 nm used in this work. In addition to the maximum absorption peak appeared around 300 nm, dye 8 also has two absorption shoulders about 375 nm and 425 nm, respectively; while dye 9 showed three absorption peaks around 400 nm, 325 nm and 275 nm, respectively. Furthermore, the extinction coefficients of these two dyes around 405 nm were summary in Table S1, e.g. $9150 \text{ M}^{-1} \text{ cm}^{-1}$ for dye 9 and $4280 \text{ M}^{-1} \text{ cm}^{-1}$ for dye 8.

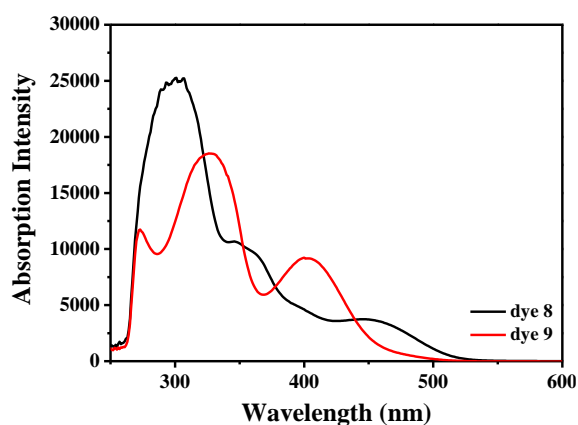


Figure 3. UV-Vis absorption spectra of dyes 8 and 9 (5×10^{-3} wt%) in water

Since Iod is not soluble in water, photolysis of these two dyes was carried out with Iod/TEA in DMSO solvent. As shown in Figure S2, absorption intensity of the characteristic peaks of the dye 8 based one-/two-/three-component photoinitiating

systems (dye 8, dye 8-Iod, dye 8-TEA, dye 8-Iod-TEA) at 350 nm dropped with light irradiation, while the absorption intensity of the other peak near 450 nm increased steadily. This indicated that some new products were generated during the photolysis process. Moreover, although the combination of dye 8 with Iod and TEA reached the highest dye consumption during the whole photolysis process, the consumption value was still low (only about 26%).

Interestingly, there was no significant photolysis activity for dye 9 in the presence of Iod, and only the absorption intensity at 340 nm was reduced upon light irradiation at LED@405nm (see Figure 4). However, substantial changes were observed in the absorption spectra of dye 9 alone or dye 9 with Iod and amine, and their photolysis (irradiation time 10 min) was faster than that of dye 8 (irradiation time \cong 60 min), due to its greater molar extinction coefficient at 405 nm (see Table S1). Furthermore, throughout the photolysis process, the absorption intensity of two characteristic absorption peaks around 280 nm and 400 nm decreased with light irradiation, except for a new absorption peak at 340 nm, where the absorption intensity gradually increased.

Furthermore, -the obvious photolysis process of the two characteristic absorption peaks at around 280 nm and 400 nm could be clearly observed after the addition of amine to a solution of dye 9. In addition, two new absorption peaks appeared at 340 and 500 nm, and their absorption intensity gradually increased with continuous irradiation, accompanied by a red-shift phenomenon. Figure S3 shows that the consumption of dye 9 reached by the three-component PIS (dye 9/Iod/amine) was slightly higher than that of the two-component PIS based on dye 9/amine combinations, which are both close to 80% and much higher than the values achieved with dye 9 alone (e.g. consumption of about 50%). Except for dye 9 and Iod, the consumption of the other three groups is significantly higher than that achieved by each group of dye 8, which is compatible with their photoinitiation ability shown in [Figure 2](#).

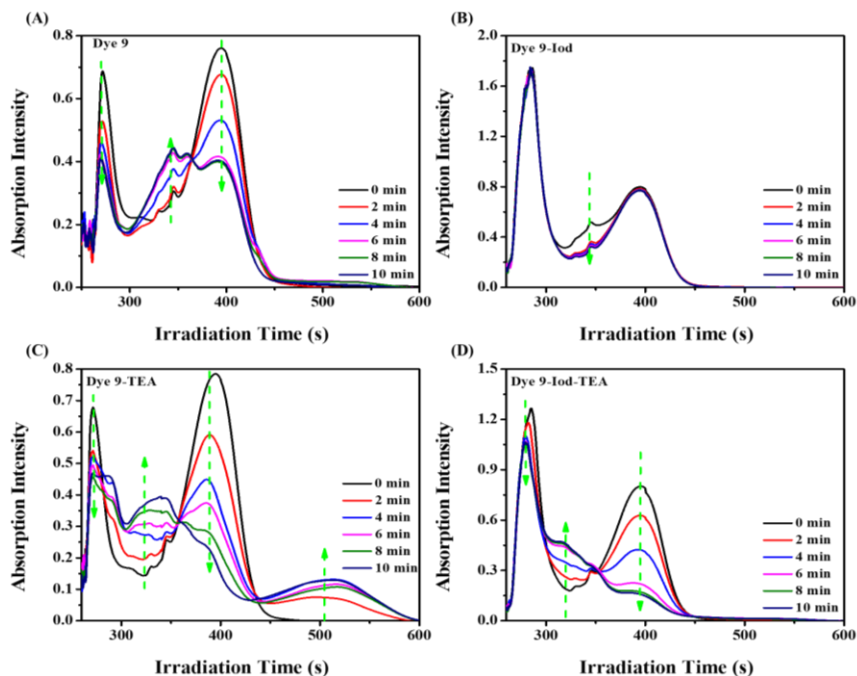


Figure 4. Photolysis of dye 9 based one/two/three-component systems (dye 9, dye 9-Iod, dye 9-TEA, dye 9-Iod-TEA) in DMSO under LED@405nm.

Fluorescence quenching of dye 9 was also performed in DMSO to demonstrate the feasibility of the interactions between dye 9 and Iod/amine. Emission peak of dye 9 appeared at 500 nm, and its intensity steadily dropped after the addition of Iod/amine. Remarkably, the fluorescence quenching process between dye 9 and Iod/amine was depicted as non-linear curvature (shown in Figure 5), which seems more probable that the two quenching mechanisms static and dynamic quenching contributed simultaneously [40]. These results demonstrated that both Iod and amine could be utilized as excellent quenchers for dye 9.

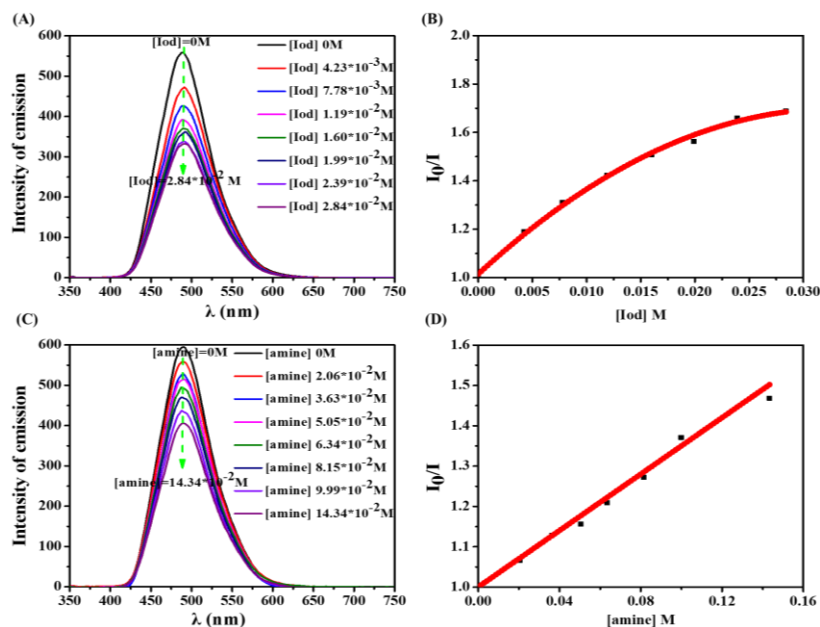


Figure 5. Fluorescence spectrum of the fluorescence quenching process between (A)(B) dye 9 with Iod and (C)(D) dye 9 with amine

To further understand the interactions existing between dye and Iod/amine, the free energy changes of the electron transfer processes ($\Delta G_{\text{Iod}}/\Delta G_{\text{EDB}}$) described in [Scheme 3](#) were also examined. First, energy of the first excited singlet state (E_{S1}) was estimated by crossing the standardized absorption spectra with the fluorescence spectra obtained in DMSO (see Table 3 and Figure S4). Oxidation and reduction potentials of dye 9 in DMSO were then evaluated using cyclic voltammetry. As shown in Figure S5, their oxidation and reduction peaks were quite minor due to the influence of the solvent. Finally, according to the above parameters, the free energy changes of the electron transfer reactions between the dye and the Iod/amine are all negative, indicating that the electron transfer process between the dye and the two additives Iod/amine may occur, proving the practicality of the involved mechanisms outlined in [Scheme 3](#).

elsewhere [42], the hyperfine coupling constant determined by simulated spectra (Figure 6C and D) revealed the formation of phenyl radical ($a_N = 14.8$ G and $a_H = 2.6$ G).

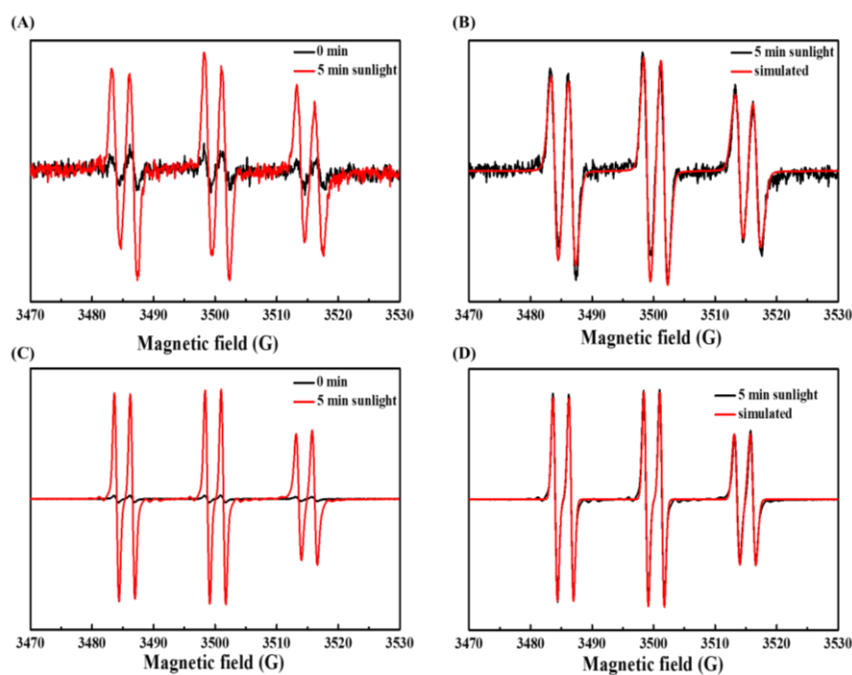


Figure 6. ESR spectra of (A) dye 9-TEA with irradiation time = 0 min (black), 5 min under sunlight; (B) dye 9-TEA system with irradiation time = 5 min (black) and simulated (red) spectra; (C) dye 9-Iod system with irradiation time = 0 min (black) and 5 min (red); (D) dye 9-Iod system with irradiation time = 5 min (black) and simulated (red) spectra.

3.4 Preparation of silver nanoparticles (AgNPs)

In this study, the proposed water-soluble dyes and additives (Iod/amine) were irradiated at LED@405 nm to generate a series of radicals and cations *via* a series of redox reactions (as shown in Scheme 3), mainly initiating the polymerization of PEG-DA monomers, as well as contributing to the *in-situ* reduction of AgNO_3 to AgNPs. As shown in Figure 7(A), absorbance of the characteristic peak of silver nanoparticles at 420 nm [43] in DMF solution increased with the sustained light irradiation, indicating that the proposed photoinitiating system (*i.e.* dye 9/Iod/TEA)

could reduce Ag^+ to AgNPs [41]. During the irradiation process, color of the solution changed from light yellow to dark yellow, and a coating of silver nanoparticles was visible on one side of the cuvette after 100 min of light irradiation (see Figure 7(B)). Nothing was observed by TEM before the light exposure, while after 100 min of light irradiation, the generated silver nanoparticles were uniformly distributed in the DMF solution in the form of round spheres with a size of about 7 nm, accompanied by a small number of nanoparticles aggregated in the form of larger spheres with a size of about 20 nm (see Figure S6(A)). Due to the polarity of the water and the effect of sunlight, a large number of particles with a size of about 10-20 nm can be observed in the aqueous solution prior to exposure to LED@405nm, (see Figure 7(C) and S6(B)); however, after irradiated for 30 min, the color of the solution deepened, and the particles increased and agglomerated in irregular shapes (see Figure 7(C) and S6(C)). Furthermore, we used RT-FTIR to investigate the influence of the presence of different concentrations of silver ions on the photopolymerization efficiency of PEG-DA aqueous monomer. Figure 7(D) shows that the inclusion of a tiny amount of silver ions ($\leq 1\%$) had no significant effect on the polymerization of PEG hydrogels, which may be deep-cured within 100 s with a final acrylate functional conversion of about 99%. When the concentration of silver ions was raised to 8%, polymerization efficiency of PEGDA monomers decreased noticeably, and the final functional conversions dropped to 55%, owing to the competition between the polymerization of PEGDA monomers and the reduction of Ag^+ to AgNPs. Furthermore, the solution darkened with increasing silver ion concentration, impeding the light penetration. The upper surface of the produced PEG hydrogel was covered with silver nanoparticles, whereas the silver nanoparticles on the bottom surface were less and aggregated into clusters due to the influence of light penetration (see Figure S6 (D-E)).

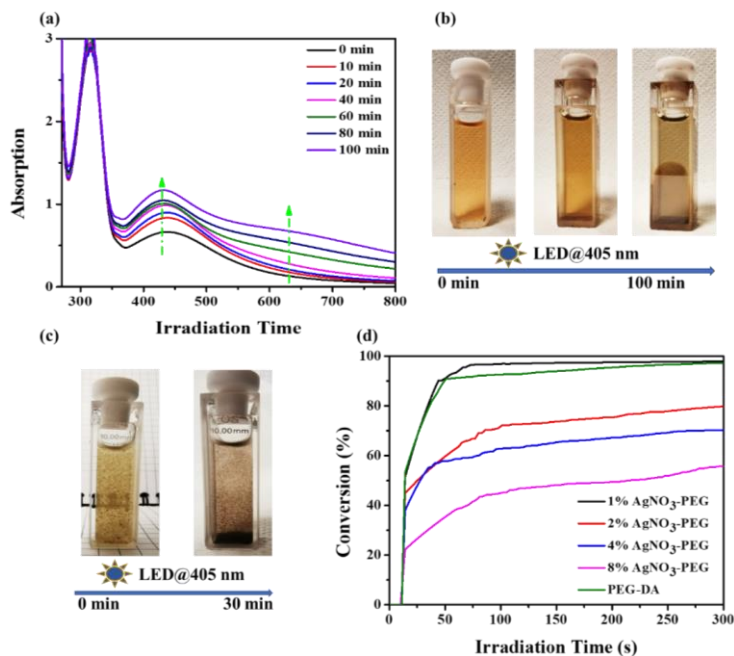


Figure 7. (A) In-situ photochemical preparation of AgNPs with 0.1 wt% dye8-1.5 wt% TEA-1.5 wt% Iod (0.1 wt%) and AgNO₃ (4 wt%) in DMF followed by UV-Vis absorption spectroscopy in air atmosphere; (B) The color changes of DMF containing 0.1 wt% dye8-1.5 wt% TEA-1.5 wt% Iod (0.1 wt%) and AgNO₃ (4 wt%) after 100 mins light irradiation; (C) The color changes of water containing 0.1 wt% dye8-1.5 wt% TEA-1.5 wt% Iod (0.1 wt%) and AgNO₃ (4 wt%) after 30 mins light irradiation; (D) Photopolymerization kinetics of dye 9 with the additive (1.5 wt% TEA/L-Arg and 1.5 wt% Iod) and different concentration of AgNO₃ in the monomer of PEG-SR 610 (50 wt%)-water(50 wt%) upon LED@405 nm irradiation. (thickness is about 2 mm) and the irradiation starts from $t = 10$ s.

3.5. Mechanical properties of obtained hydrogels.

Photoinitiation ability of the water-soluble dyes-based PIS was further explored by measuring the change in storage (G') modulus during the formation of hydrogels *via* photopolymerization using a Haake-Mars rotational photo rheometer with time-scan experiments, the irradiation starts at $t = 20$ s and the results are presented in Figure 8(A). In comparison to the commercially available water-soluble UV photoinitiator I2959,

the water-soluble photoinitiating system not only exhibited higher water solubility but also was appropriate for visible light and demonstrated better photopolymerization efficiency (slope of the curve, the larger the slope the higher the polymerization efficiency). Within 100 s, all three-component PIS based on dyes 8 and 9 were able to complete the phase transition and reached the maximum storage modulus (G'). PIS based on dye 9 demonstrated a much higher polymerization efficiency than that of dye 8 based PIS. Effect of varying the silver ion concentrations on the polymerization efficiency under visible light was further investigated. Addition of 1 wt%, 2 wt%, and 4 wt% silver ions had no effect on the ultimate storage modulus (G') of the fabricated hydrogels; however, the polymerization efficiency of the photosensitive formulations reduced dramatically with increasing silver ion concentration.

Furthermore, as shown in Figure 8(B), the PEG hydrogels produced with I2959 reached a 10% elongation strain, equivalent to tensile fracture energy of roughly 0.9 MPa. Under visible light irradiation, the elongation and the corresponding fracture potential of the PEG hydrogels prepared with the PIS based on water-soluble dyes were lower than those prepared with I2959, with the exception of the dye 9-Iod- TEA based PIS, which the elongation of the hydrogels prepared reached 13%. FTIR results showed that there was no significant difference in the photopolymerization efficiency of the water-soluble PIS consisting of L-Arg or TEA as amines paired with Iod and dye. However, TEA was eventually chosen as the electron donor (amine) due to its better stability and water solubility than L-arg. Subsequently, the tensile properties of dye-Iod-TEA and dye-Iod-L-Arg-initiated hydrogels were studied, and the results demonstrated that the hydrogels prepared from dye-Iod-TEA displayed longer elongation strain and higher fracture potentials, proving that TEA is more suitable to be used as an electron donor. Furthermore, the stretching properties of the dye 9-based hydrogels were much better than those of dye-8, which corresponded to the superior photoinitiation ability of the dye-9-based PIS. More crucially, with the addition of silver ions, the dye-Iod-TEA based PIS initiated free-radical photopolymerization and also reduced the silver cations to silver nanoparticles. These two processes competed with each other, resulting in a considerable drop in the polymerization efficiency of the photosensitized formulations and a steady weakening of the tensile properties of the produced hydrogels with increasing silver ion concentration.

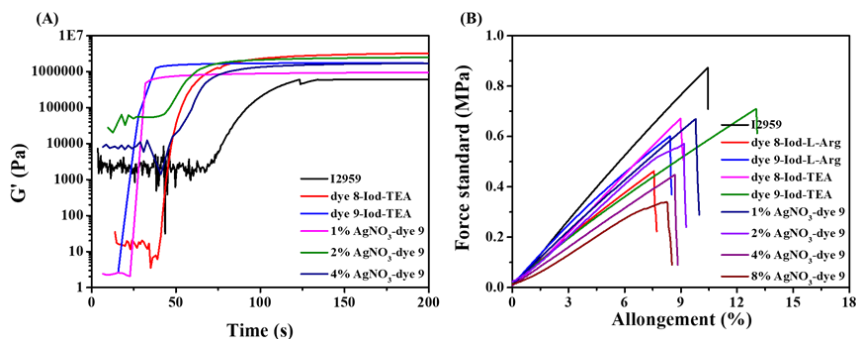


Figure 8. (A) The storage (G') modulus of hydrogels during the photopolymerization process initiated with 0.5 wt% I2959 and dyes-based three-component PIS with/without AgNO_3 ; (B) Tensile property of hydrogels obtained with 0.5 wt% I2959 and dyes-based three-component PIS with/without AgNO_3 .

3.6 Applications in 3D and 4D printing.

Since dyes 8 and 9 /Iod/TEA-based PISs displayed excellent photopolymerization efficiencies under visible light irradiation, laser write experiments were directly carried out to fabricate the PEG-hydrogels. The sensitive formulations were effectively written to generate stable 3D hydrogels, as illustrated in Figure 9. In comparison to the dye 8/Iod/amine-based PIS, the dye 9/Iod/amine-based formulation needed a reduced irradiation time (~ 1 min) to achieve a 3D pattern with a thickness of roughly 2.3 mm. In addition, incorporation of AgNO_3 to the formulation required a longer irradiation time (~ 5 min) to obtain 3D patterns whose thickness decreased into 1.9 mm (see Figure 9(C-D)), demonstrating that the presence of AgNO_3 significantly reduced the polymerization efficiency of PEGDA, which was in full agreement with the results obtained for free radical polymerization.

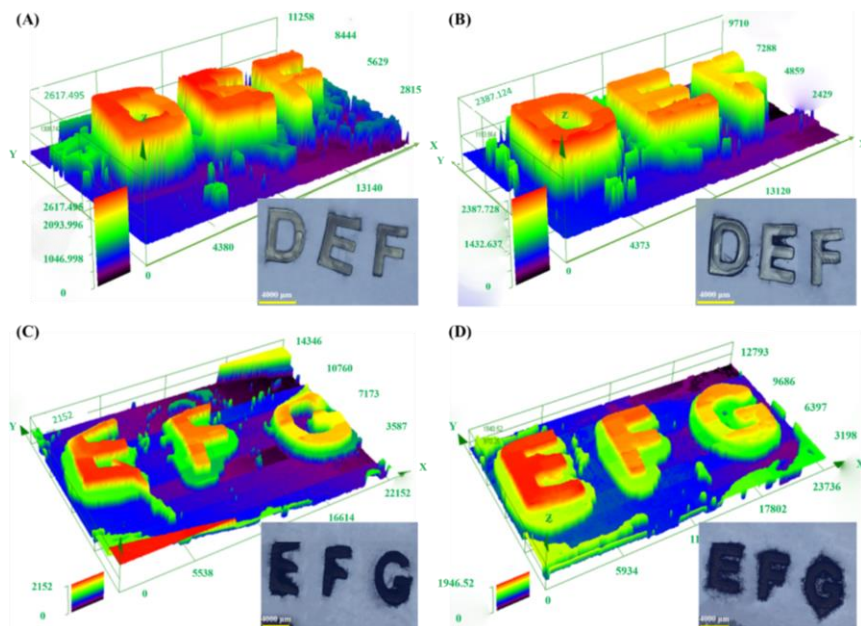


Figure 9. 3D morphologies of the 3D patterns obtained through the direct laser write experiment initiated with proposed water-soluble dyes-based PIS in PEG-DA aqueous monomer characterized by numerical optical microscope: (A) initiated by dye 8-Iod-TEA; (B) initiated by dye 9-Iod-TEA; (C) initiated by dye 8-Iod-TEA with 4 wt% AgNO_3 ; (D) initiated by dye 9-Iod-TEA with 4 wt% AgNO_3 .

Since the water content of the monomer used was about 50 wt%, the swelling properties of the obtained four kinds of PEG-hydrogels were investigated using two methods: direct immersion in water until swelling equilibrium was reached as well as dehydration to remove the internal water before immersion in water. The swelling ratio of each group of hydrogels was calculated by comparing their initial wet weight to the wet weight after attaining the swelling equilibrium, and the result was shown in Figure 10. PEG hydrogels initiated by dye 8-based PIS exhibited an improved hydrophilicity during swelling in water after dehydration, with the swelling ratio increasing from 35% achieved from the direct swelling process to 55%. However, the immediately swollen process of PEG hydrogel prepared by the dye 9 based PIS displayed greater hydrophilicity, with a swelling ratio of about 70%, which is much higher than that of post-dehydration swelling (~57%). Furthermore, introduction of AgNPs into PEG hydrogels also reduced their hydrophilicity (e.g. the swelling ratio of PEG hydrogels

prepared by dye 9/Iod/amine decreased from 70% to 35%). Figure 11 and Table S2 clearly show that the morphology and the volume of the PEG-hydrogel also changed significantly during these two swelling processes.

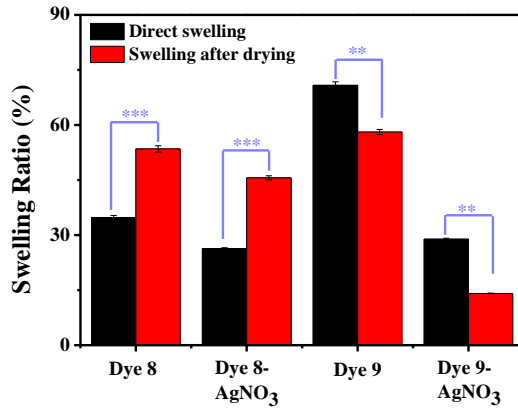


Figure 10. Swelling ratio of PEG hydrogels and AgNPs contained PEG hydrogels initiated with water-soluble dyes 8 and 9 based PIS obtained by two swelling routes.

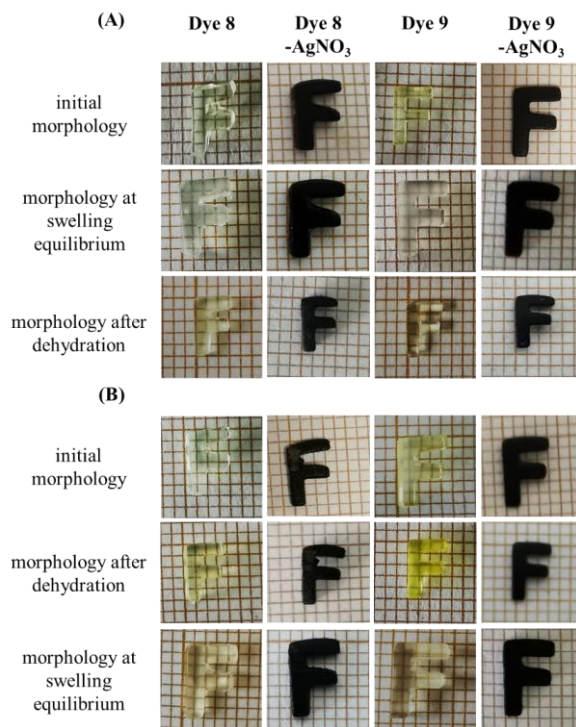


Figure 11. Photos of PEG hydrogels and AgNPs contained PEG hydrogels during the swelling process: route 1 - initial morphology, morphology at swelling equilibrium and morphology after dehydration; route 2 - initial morphology, morphology after dehydration, and morphology at swelling equilibrium

3.7 Antibacterial activity of hydrogels with different content of AgNPs.

Numerous studies have demonstrated that AgNPs have broad antibacterial activities and represent a new generation of antibacterial agents [44-46]. Therefore, in this work, *Escherichia coli* was selected to study the antibacterial effect of the prepared AgNPs-containing PEG hydrogels. Initially, the culture of *E. coli* was carried out in solid LB-agar, pure PEG hydrogel was used as the control group, and hydrogels with different contents were used as the experimental group. A halo of growth inhibition was clearly observed only around the hydrogels of the experimental group (see Figure 12(A)). Second, in order to determine the effect of different contents of AgNPs-PEG hydrogels on the antibacterial effect, we calculated the area of the antibacterial ring of each group, as shown in Figure 12(B), with the increase of AgNPs content, its antibacterial activity also increased. Considering the polymerization efficiency of the hydrogels with different contents of silver nanoparticles and the mechanical properties of the prepared hydrogels, AgNPs-containing PEG-hydrogels prepared with 4% AgNO₃ were finally selected as the best combination for the preparation of antibacterial material.

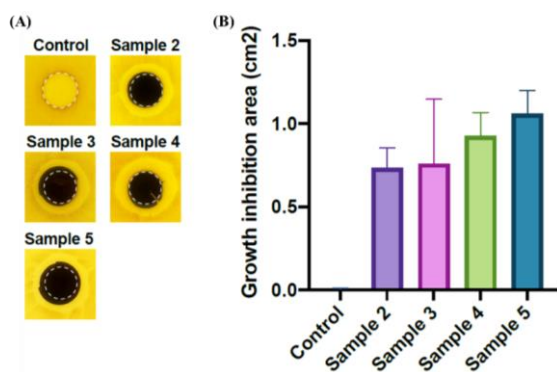


Figure 12. (A) Pictures of *Escherichia coli* in presence of PEG, AgNPs contained PEG pellet during the overnight culture at 37°C; (B) the areas of halo of growth inhibition appeared around different content of AgNPs contained PEG pellet. (PEG hydrogel-control; 1% AgNPs contained PEG hydrogel -sample 1; 2% AgNPs

contained PEG hydrogel - sample 2; 4% AgNPs contained PEG hydrogel - sample 3; 8% AgNPs contained PEG hydrogel - sample 4).

4. Conclusions

In this research, a series of new naphthalimide derivatives that can be used for the 3D printing of hydrogels was prepared to address the challenge of developing highly efficient water-soluble PIs in the UV-visible region. The prepared two naphthalimide potassium salts (dyes 8 and 9) not only showed water solubility far beyond that of the commercially available PI (I2959), but also achieved extremely high polymerization efficiency when used in combination with a co-initiator (Iod/amine) under visible light irradiation. We fabricated hydrogel scaffolds with high resolution using an SLA-based 3D printer, and they exhibited better mechanical properties than the hydrogels prepared from the photoinitiator I2959. The advantage of the proposed dyes-based aqueous PIS is the high photoinitiation efficiency for aqueous monomer PEG-DA while reducing Ag^+ to AgNPs to prepare the antibacterial hydrogels, where the optimal antibacterial concentration of silver nitrate used was 4 wt%. In conclusion, our developed aqueous PIs showed better performance than the existing commercial aqueous PI I2959, thus offering various new possibilities for a wide range of applications.

Supplementary Materials: The following Supporting Information is available online. Figure S1. The photos of different concentrations of dyes 8 and 9 in water. Figure S2. The photolysis of dye 8 based one/two/three-component photoinitiating systems. Figure S3. The consumption of dyes 8 and 9 during the photolysis process. Figure S4. The normalized absorption and emission spectrums of dyes 8 and 9 in water. Figure S5. The Cyclic Voltammetry of dyes 8 and 9 was determined in DMSO. Figure S6. The TEM and SEM of AgNPs generated in DMF, in water, and within PEG-hydrogels. Table S1. The volume changes during the swelling process. The synthesis of different 11 kinds of naphthalimide derivatives.

Funding: This research project is supported by China Scholarship Council (CSC) (201906280059) and the Australian Research Council (FT170100301).

Institutional Review Board Statement: not applicable

Informed Consent Statement: not applicable

Data Availability Statement: No samples available.

Acknowledgments: This research project is supported by China Scholarship Council (CSC) (201906280059). P.X. acknowledges funding from the Australian Research Council (FT170100301).

Conflicts of Interest: The authors declare no conflict of interest.

References:

1. Zhou, H.; Bhaduri, S.B. Multimaterial 3D Printing Technology. Chapter 12-3D printing in the research and development of medical devices. Editor(s): Yang, J.Q.; Li, N.; Shi, J.Q.; Tang, W.L.; Zhang, G.; Zhang, F. *Biomaterials in Translational Medicine*. 2019, 269-289.
2. Guidance, F.D.A. Technical Considerations for Additive Manufactured Medical Devices. Food and Drug Administration: New Hampshire, NH, USA. 2017.
3. Berman, B. 3D printing: the new industrial revolution. *Bus. Horiz.* 2012;55(2), 155-162.
4. Tumbleston, J.R.; Shirvanyants, D.; Ermoshkin, N.; Janusziewicz, R.; Johnson, A.R.; Kelly, D.; Chen, K.; Pinschmidt, R.; Rolland, J.P.; Ermoshkin, A.; Samulski, E.T. Continuous liquid interface production of 3D objects. *Science* 2015, 347, 1349-1352.
5. Hong, S.; Sycks, D.; Chan, H.F.; Lin, S.; Lopez, G.P.; Guilak, F.; Leong, K.W.; Zhao, X. 3D printing of highly stretchable and tough hydrogels into complex, cellularized structures. *Adv. Mater.* 2015, 27, 4035-4040.
6. Aabith, S.; Akilbekova, D.; Capelli, C.; Chameettachal, S.; Das, A.K.; Fang, F.H.; Gaisford, S.; Homer-Vanniasinkam, S.; Jadhav, R.G.; Kalaskar, D.M.; Mektepbayeva, D.; Nommeots-Nomm, A.; Pati, F.; Poologasundarampillai, G.; Provaggi, E.; Rath, S.N.; Roopavath, U.K.; Sankar, S.; Schievano, S.; Tiwari, M.K. Editor(s): Kalaskar, D.M. 3D Printing in Medicine, Woodhead Publishing, 2017.
7. Wagner, S.M.; Walton, R.O. Additive manufacturing's impact and future in the aviation industry, *Prod. Plan. Control.* 2016, 27(13), 1124-1130.

8. Ford, S.; Minshall, T. Where and how 3D printing is used in teaching and education. *Addit. Manuf.* 2019, 25, 131-150.
9. Canessa, E.; Fonda, C.; Zennaro, M.; Deadline, N. Low-cost 3D printing for science, education and sustainable development. *Low-Cost 3D Printing*. 2013, 11(1).
10. Peppas, N.A.; Hoffman, A.S. Hydrogels. *Biomater. Sci.* 2020,153-166.
11. Lee, K.Y.; Mooney, D.J. Hydrogels for tissue engineering. *Chem. Rev.* 2001, 101(7), 1869-1880.
12. Zhang, Y.S.; Khademhosseini, A. Advances in engineering hydrogels. *Science* 2017, 356 (6337), 1-10.
13. Distler, T.; Boccaccini, A.R. 3D printing of electrically conductive hydrogels for tissue engineering and biosensors—A review. *Acta. Biomater.* 2020, 101,1-13.
14. Saroia, J.; Yanen, W.; Wei, Q.; Zhang, K.; Lu, T.; Zhang, B. A review on biocompatibility nature of hydrogels with 3D printing techniques, tissue engineering application and its future prospective. *Bio-Des. Manuf.* 2018, 1(4), 265-279.
15. Hong, H.; Seo, Y.B.; Lee, J.S.; Lee, Y.J.; Lee, H.; Ajiteru, O.; Sultan, M.T.; Lee, O.J.; Kim, S.H.; Park, C.H. Digital light processing 3D printed silk fibroin hydrogel for cartilage tissue engineering. *Biomaterials* 2020, 232, 119679.
16. Mu, X.; Fitzpatrick, V.; Kaplan, D.L. From silk spinning to 3D printing: Polymer manufacturing using directed hierarchical molecular assembly. *Adv. Healthc. Mater.* 2020, 9(15), 1901552.

17. Williams, C.G.; Malik, A.N.; Kim, T.K.; Manson, P.N.; Elisseeff, J.H. Variable cytocompatibility of six cell lines with photoinitiators used for polymerizing hydrogels and cell encapsulation. *Biomaterials* 2005, *26*(11), 1211-1218.
18. Fairbanks, B.D.; Schwartz, M.P.; Bowman, C.N.; Anseth, K.S. Photoinitiated polymerization of PEG-diacrylate with lithium phenyl-2, 4, 6-trimethyl-benzoylphosphinate: polymerization rate and cytocompatibility. *Biomaterials* 2009, *30*(35), 6702-6707.
19. Lin, H.; Zhang, D.; Alexander, P.G.; Yang, G.; Tan, J.; Cheng, A.W.M.; Tuan, R.S. Application of visible light-based projection stereolithography for live cell-scaffold fabrication with designed architecture. *Biomaterials* 2013, *34*(2), 331-339.
20. Tomal, W.; Ortyl, J. Water-soluble photoinitiators in biomedical applications. *Polymers* 2020, *12*(5), 1073.
21. Nguyen, A.K.; Gittard, S.D.; Koroleva, A.; Schlie, S.; Gaidukeviciute, A.; Chichkov, B.N.; Narayan, R.J. Two-photon polymerization of polyethylene glycol diacrylate scaffolds with riboflavin and triethanolamine used as a water-soluble photoinitiator. *Regen. Med.* 2013, *8*(6), 725-738.
22. Kim, S.H.; Chu, C.C. Visible light induced dextran-methacrylate hydrogel formation using (-)-riboflavin vitamin B2 as a photoinitiator and L-arginine as a co-initiator. *Fibers. Polym.* 2009, *10*(1), 14-20.
23. Kim, S.H.; Chu, C.C. Fabrication of a biodegradable polysaccharide hydrogel with riboflavin, vitamin B2, as a photo-initiator and L-arginine as coinitiator upon UV irradiation. *J. Biomed. Mater. Res. Part. B. Appl. Biomater.* 2009, *91*(1), 390-400.
24. Zhang, T.; Yeow, J.; Boyer, C. A cocktail of vitamins for aqueous RAFT polymerization in an open-to-air microtiter plate. *Polym. Chem.* 2019, *10*(34), 4643-4654.

25. Benedikt, S.; Wang, J.; Markovic, M.; Moszner, N.; Dietliker, K.; Ovsianikov, A.; Liska, R. (2016). Highly efficient water-soluble visible light photoinitiators. *J. Polym. Sci. A. Polym. Chem.* 2016,54(4), 473-479.
26. Rahal, M.; Mokbel, H.; Graff, B.; Pertici, V.; Gimes, D.; Toufaily, J.; Hamieh, T.; Dumur, F.; Lalevée, J. Naphthalimide-Based dyes as photoinitiators under visible light irradiation and their applications: Photo-composite synthesis, 3D printing and polymerization in water. *Chem. Photo. Chem.* 2021, 5(5), 476-490.
27. Ott, I.; Xu, Y.; Liu, J.; Kokoschka, M.; Harlos, M.; Sheldrick, W. S.; Qian, X. Sulfur-substituted naphthalimides as photoactivatable anticancer agents: DNA interaction, fluorescence imaging, and phototoxic effects in cultured tumor cells. *Bioorgan. Med. Chem.* 2008, 16(15), 7107-7116.
28. Xiao, P.; Dumur, F.; Zhang, J.; Graff, B.; Morlet-Savary, F.; Fouassier, J. P.; Lalevée, J. Naphthalic anhydride derivatives: Structural effects on their initiating abilities in radical and/or cationic photopolymerizations under visible light. *J. Polym. Sci. A. Polym. Chem.* 2015, 53(24), 2860-2866.
29. Li, C.; Wang, Y.; Huang, S.; Zhang, X.; Kang, X.; Sun, Y.; Liu, Y. A photostable fluorescent probe for long-time imaging of lysosome in cell and nematode. *Talanta.* 2018, 188, 316-324.
30. Ong, J. X.; Ang, W. H. Development of a pre-assembled through-bond energy transfer (TBET) fluorescent probe for ratiometric sensing of anticancer platinum (II) complexes. *Chem. Asian. J.* 2020, 15(9), 1449-1455.
31. Rahal, M.; Mokbel, H.; Graff, B.; Pertici, V.; Gimes, D.; Toufaily, J.; Lalevée, J. Naphthalimide-based dyes as photoinitiators under visible light irradiation and their applications: photocomposite synthesis, 3D printing and polymerization in water. *Chem. Photo. Chem.* 2021, 5(5), 476-490.

32. Scherzer, T. Photopolymerization of acrylates without photoinitiators with short-wavelength UV radiation: A study with real-time Fourier transform infrared spectroscopy[J]. *J. Polym. Sci. A. Polym. Chem*, 2004, 42(4), 894-901.
33. Soltani, T.; Entezari M H. Photolysis and photocatalysis of methylene blue by ferrite bismuth nanoparticles under sunlight irradiation. *J. Mol. Catal. A. Chem.* 2013, 377, 197-203.
34. Watanabe, T.; Yoshida, M.; Fujiwara, S.; Abe, K.; Onoe, A.; Hirota, M.; Igarashi, S. Spin trapping of hydroxyl radical in the troposphere for determination by electron spin resonance and gas chromatography/mass spectrometry. *Anal. Chem.* 1982, 54(14), 2470-2474.
35. Maldonado-Codina, C.; Efron, N. Impact of manufacturing technology and material composition on the mechanical properties of hydrogel contact lenses. *Ophthalmic. Physiol. Opt.* 2004, 24(6): 551-561.
36. Lee, S.J.; Heo, M.; Lee, D.; Han, S.; Moon, J.H.; Lim, H.N.; Kwon, I.K. Preparation and characterization of antibacterial orthodontic resin containing silver nanoparticles. *Appl. Surf. Sci.* 2018, 432, 317-323.
37. Omidian, H.; Hasherni, S. A.; Askari, F.; Nafisi, S. Swelling and crosslink density measurements for hydrogels. *Iranian J. of Polymer Science and Technology.* 1994, 3(2), 115-119.
38. Bundjaja, V.; Santoso, S.P.; Angkawijaya, A.E.; Yuliana, M.; Soetaredjo, F.E.; Ismadji, S.; Ayucitra, A.; Gunarto, C.; Ju, Y.H.; Ho, M.H. Fabrication of cellulose carbamate hydrogel-dressing with rarasaponin surfactant for enhancing adsorption of silver nanoparticles and antibacterial activity. *Mater. Sci. Eng. C.* 2021, 118, 111542.
39. Chen, H.; Regeard, C.; Salmi, H.; Morlet-Savary, F.; Giacoletto, N.; Nechab, M.; Lalevéé, J. Interpenetrating polymer network hydrogels using natural based dyes

initiating systems: Antibacterial activity and 3D/4D performance. *Eur. Polym. J.* 2022, *166*, 111042.

40. Blatt, E.; Chatelier, R.C.; Sawyer, W.H. Effects of Quenching Mechanism and Type of Quencher Association on Stern-Volmer Plots in Compartmentalized Systems. *Biophys. J.* 1986, *50*(2), 349-356.
41. Qi, Y.; Li, H.; Fouassier, J.P.; Lalevée, J.; Sheridan, J.T. Comparison of a new photosensitizer with Erythrosin B for use in a photopolymer. In Holography: Advances and Modern Trends IV. *International Society for Optics and Photonics.* 2015, 9508, 95080I.
42. Tehfe, M. A.; Dumur, F.; Graff, B.; Morlet-Savary, F.; Fouassier, J. P.; Gimes, D.; & Lalevee, J. New push-pull dyes derived from michler's ketone for polymerization reactions upon visible lights. *Macromolecules* 2013, *46*(10), 3761-3770.
43. Du, L.; Xu, Q.; Huang, M.; Xian, L.; & Feng, J. X. Synthesis of small silver nanoparticles under light radiation by fungus *Penicillium oxalicum* and its application for the catalytic reduction of methylene blue. *Mater. Chem. Phys.* 2015, *160*, 40-47.
44. López-Heras, M.; Theodorou, L.G.; Leo, B.F.; Ryan, M.P.; Porter, A.E. Towards understanding the antibacterial activity of Ag nanoparticles: electron microscopy in the analysis of the materials-biology interface in the lung. *Environ. Sci.: Nano*, 2015, *2*, 312-326.
45. Nigussie, G.Y.; Tesfamariam, G.M.; Tegegne, B.M.; Weldemichel, Y.A.; Gebreab, T.W.; Gebrehiwot, D.G.; Gebremichel, G.E. Antibacterial activity of Ag-doped TiO₂ and Ag-doped ZnO nanoparticles. *Int. J. Photoenergy.* 2018.
46. Sotiriou, G. A.; Teleki, A.; Camenzind, A.; Krumeich, F.; Meyer, A.; Panke, S.; Pratsinis, S. E. Nanosilver on nanostructured silica: Antibacterial activity and Ag surface area. *Chem. Eng. J.* 2011, *170*(2-3), 547-554.